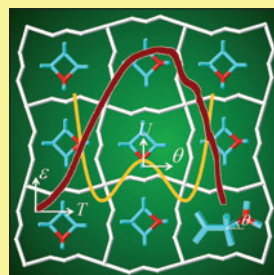
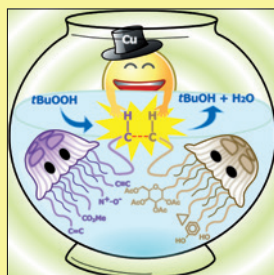
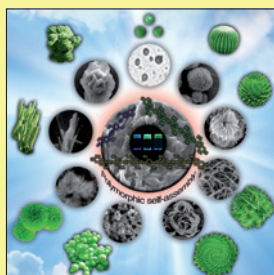
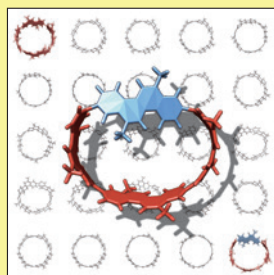
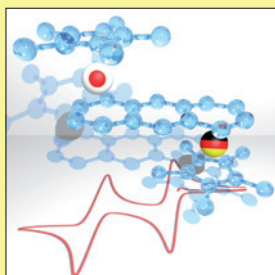
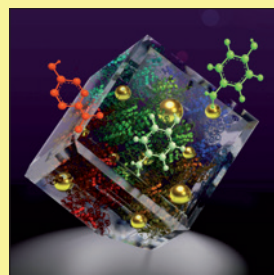
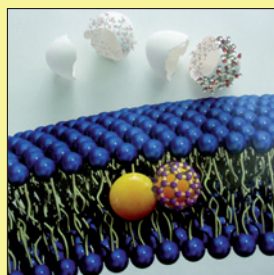
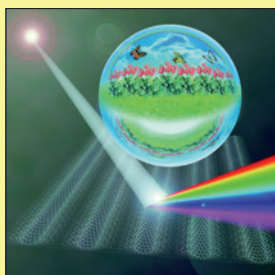


# CHEMISTRY

## AN **ASIAN** JOURNAL



# REPRINT

An **ACES** journal

WILEY-VCH

A Journal of



[www.chemasianj.org](http://www.chemasianj.org)

# CHEMISTRY

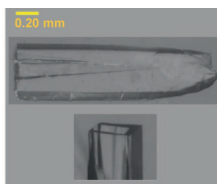
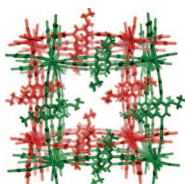
---

## AN **ASIAN** JOURNAL

### REPRINT

#### Metal–Organic Frameworks

#### Metal–Organic Frameworks Incorporating Various Alkoxy Pendant Groups: Hollow Tubular Morphologies, X-ray Single-Crystal Structures, and Selective Carbon Dioxide Adsorption Properties



**Bigger on the inside:** Macrosized, hollow, tubular single crystals of a series of 3D porous metal–organic frameworks (MOFs) with various alkoxy substituents ( $-\text{OC}_n\text{H}_{2n+1}$ ;  $n = 1-8$ ) have been synthesized and the X-ray crystal structures determined (see figure). Upon activation, the MOFs with methoxy and ethoxy pendant groups show selective  $\text{CO}_2$  adsorption over  $\text{N}_2$  and  $\text{CH}_4$  at room temperature.

*T. K. Prasad, M. P. Suh\** — 2257–2263

**Keywords:** carbon dioxide capture · crystal growth · crystal morphology · gas separation · metal–organic frameworks

**2015 – 10/10**

## Metal–Organic Frameworks

## Metal–Organic Frameworks Incorporating Various Alkoxy Pendant Groups: Hollow Tubular Morphologies, X-ray Single-Crystal Structures, and Selective Carbon Dioxide Adsorption Properties

Thazhe Kootteri Prasad and Myunghyun Paik Suh<sup>\*,[a]</sup>

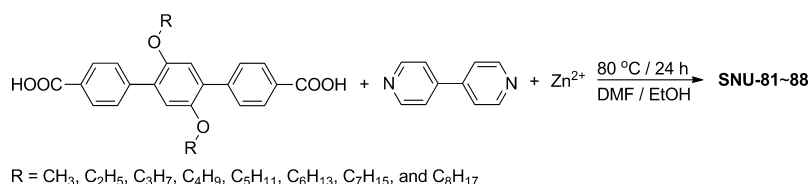
**Abstract:** Eight porous metal–organic frameworks (MOFs) incorporating various alkoxy pendant groups ( $-\text{OC}_n\text{H}_{2n+1}$ ;  $n = 1-8$ ) in the channels have been synthesized. All MOFs have macrosized, hollow, single-crystal morphologies independent of the type of alkoxy pendant groups. The X-ray single-crystal structures indicate that the MOFs have doubly interpenetrated 3D frameworks that generate clover-shaped 1D channels, the window sizes of which reduce as the length of the alkoxy pendant groups increases from  $-\text{OCH}_3$  to  $-\text{OC}_8\text{H}_{17}$ . The hollow axes of the tubular crystals are parallel to the 1D

channels of the MOFs, which suggests that the hollow crystal is grown by the unidirectional addition of pillar ligands to the 2D network. Among the activated MOFs, only the MOFs with methoxy and ethoxy pendant groups show selective  $\text{CO}_2$  adsorption over  $\text{N}_2$  and  $\text{CH}_4$ , whereas those with longer alkoxy pendant groups barely adsorb  $\text{CO}_2$  at room temperature, which implies that the pendant doors of the MOFs should have an appropriate length for selective  $\text{CO}_2$  capture.

## Introduction

Metal–organic frameworks (MOFs) have potential applications in gas storage and separation, catalysis, sensing, and so forth.<sup>[1]</sup> In particular, MOFs that can be applied to the separation of  $\text{CO}_2$  from landfill and industrial flue gas have attracted a great deal of attention.<sup>[1b,2]</sup> Previously, we demonstrated that highly flexible 3D networks with small pores showed selective  $\text{CO}_2$  adsorption properties over other gases, such as  $\text{N}_2$ ,  $\text{H}_2$ , and  $\text{CH}_4$ .<sup>[2a,3]</sup> This is because the  $\text{CO}_2$  molecule has a high quadrupole moment ( $-14.3 \times 10^{-40} \text{ C m}^2$ ) and polarizability ( $2.51 \times 10^{-24} \text{ cm}^3$ ),<sup>[2b]</sup> and thus,  $\text{CO}_2$  can open up the pores of the flexible networks, which are closed for other gases. In a similar respect, the introduction of flexible alkoxy or carboxyl pendant groups into MOFs offers selective  $\text{CO}_2$  adsorption properties.<sup>[3c,4]</sup> Our continued interest in the develop-

ment of MOFs that can be applied in selective  $\text{CO}_2$  capture prompted us to synthesize a series of MOFs by using ligands that incorporate alkoxy pendant groups of various lengths (Scheme 1). Interestingly, all crystals have hollow tubular morphologies, and among the series of MOFs incorporating  $-\text{OCH}_3$



**Scheme 1.** Synthesis of  $[\text{Zn}_2(\text{C}''\text{TPDC})_2(\text{bpy})]$  ( $\text{H}_2\text{C}''\text{TPDC} = 2',5'$ -dialkoxy-[1,1':4',1''-terphenyl]-4,4''-dicarboxylic acid,  $n = 1-8$  (SNU-81–SNU-88, respectively),  $\text{bpy} = 4,4'$ -bipyridine). DMF = *N,N*-dimethylformamide.

to  $-\text{OC}_8\text{H}_{17}$  pendant groups, only the MOFs with methoxy and ethoxy pendant groups showed selective  $\text{CO}_2$  adsorption properties.

In MOF chemistry, apart from the porosity of MOFs, sometimes morphologies are important because it has been reported that kinetic separation of hydrocarbons by a MOF depends on the crystal morphology of the MOF.<sup>[5]</sup> In particular, in catalysis, the crystal faces affect the accessibility of a substrate to the interior parts of the catalysts.<sup>[6]</sup> However, studies on the morphologies of MOFs are in their infancy.<sup>[7]</sup> For microcrystalline ( $\mu\text{m}$ -sized) MOFs, unusual morphologies, such as hollow, spherical, wire-shaped, rod-like, and needle-shaped, have been reported, but their morphologies could not be controlled and were simply determined by the reaction conditions, such as temperature, reaction time, and solvents.<sup>[7,8]</sup> For macrosized

[a] Dr. T. K. Prasad, Prof. M. P. Suh<sup>†</sup>  
Department of Chemistry, Seoul National University  
Seoul 151-747 (Republic of Korea)  
E-mail: mpsuh@snu.ac.kr

[†] Current Address:  
Department of Chemistry, Hanyang University  
Seoul 133-791 (Republic of Korea)  
E-mail: mpsuh@snu.ac.kr

Supporting information for this article is available on the WWW under <http://dx.doi.org/10.1002/asia.201500332>.

(mm-sized) MOF crystals, unusual morphologies have been reported extremely rarely.<sup>[9a]</sup> It has been commonly observed that cubic networks have cubic-shaped crystals<sup>[9b]</sup> and polyhedral networks give rise to polyhedral-shaped crystals,<sup>[9c]</sup> although MOFs in low-symmetry crystal systems have never shown such relationships.

Herein, we report eight MOFs that incorporate various alkoxy pendant groups,  $[\text{Zn}_2(\text{C}^n\text{TPDC})_2(\text{bpy})]$  ( $n = 1-8$ ; SNU-81–SNU-88, respectively); all of which have macrosized, crystalline, hollow, tubular morphologies. The X-ray crystal structures of SNU-81–SNU-88 indicate that they have the same framework structures, regardless of the pendant groups, and their window sizes are reduced as the length of the alkoxy pendant increases from  $-\text{OCH}_3$  to  $-\text{OC}_8\text{H}_{17}$ . Among the MOFs, only two MOFs, with methoxy and ethoxy pendant groups, SNU-81 and SNU-82, respectively, adsorb gases at room temperature and show selective  $\text{CO}_2$  capture properties at room temperature.

## Results and Discussion

### Syntheses, Morphologies, and X-ray Crystal Structures of SNU-81–SNU-88

The solvothermal reactions of *para*-terphenyldicarboxylic acids with various alkoxy substituents ( $\text{H}_2\text{C}^n\text{TPDC}$ ;  $n = 1-8$ ),  $\text{Zn}(\text{NO}_3)_2 \cdot 6\text{H}_2\text{O}$ , and bpy, in a mixture of DMF and ethanol resulted in 3D MOFs of  $[\text{Zn}_2(\text{C}^n\text{TPDC})_2(\text{bpy})] \cdot \text{G}$  ( $n = 1-8$ ; SNU-81–SNU-88, G = guest solvent molecules). All crystals of SNU-81–SNU-88 have hollow tubular morphologies, as shown in Figure 1a. Typically, a crystal of SNU-86 has a crystal width of 0.48 mm, a hollow tube width of 0.14 mm, and wall thickness

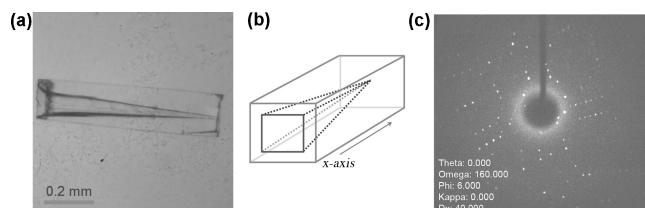


**Figure 1.** a) A hollow, tubular crystal of SNU-86-G. b) Schematic representation of the crystal morphology. c) XRD pattern of the crystal shown in a).

of 0.17 mm. The macrosized hollow-crystal morphology of a MOF has rarely been reported,<sup>[9a]</sup> although those of organic derivatives, such as nitroguanidine<sup>[10a]</sup> and sodium diethyl barbiturate,<sup>[10b]</sup> are well known. The hollow-tube width of the present SNU-86 MOF, 0.14 mm (140  $\mu\text{m}$ ), is significantly greater than that (0.01 mm, 10  $\mu\text{m}$ ) of the previously reported MOF crystal.<sup>[9a]</sup>

The single crystal XRD data of SNU-81 – SNU-88 with hollow morphologies were collected for a whole single crystal without cutting. MOFs SNU-81 – SNU-88 showed excellent single-crystal XRD patterns, even at room temperature (Figure 1c). MOFs SNU-82 – SNU-88 have very similar cell parameters, although SNU-81 has different unit cell parameters. The dicarboxylic linker in SNU-82 – SNU-88 is slightly bent, whereas that of

SNU-81 is straight. All compounds, SNU-81 – SNU-88, show isostructural doubly interpenetrated 3D networks. The structures consist of 2D square grids constructed from  $\text{Zn}_2$ -paddle-wheel units and linear dicarboxylates, with bpy pillars linking the 2D layers by coordinating at the axial sites of the paddle-wheel units. The as-formed 3D structures generate 1D clover-shaped channels that extend parallel to the *c* axis in SNU-81 and the *a*\* axis of the unit cells in SNU-82–SNU-88 (Figure 2a for the structure of SNU-82 (see also Figures S9–S10 in the Supporting

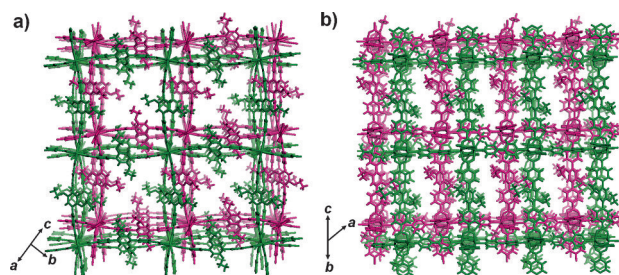


**Figure 2.** Typical views of the doubly interpenetrated structure of SNU-82: a) seen on the (100) plane, and b) seen on the  $(-111)$  plane.

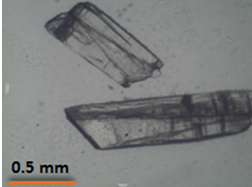
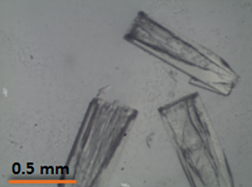
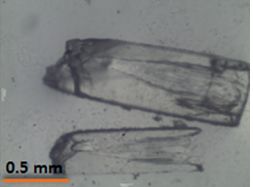
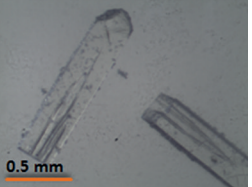
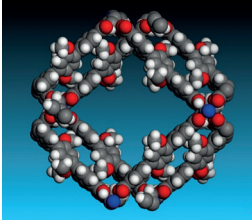
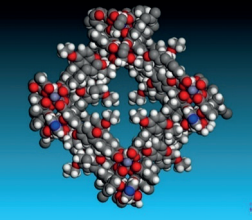
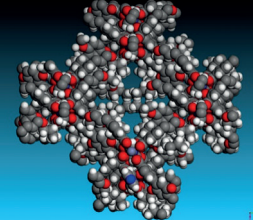
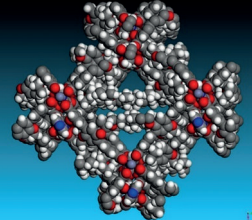
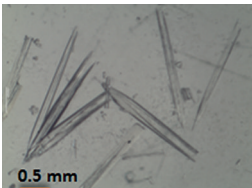
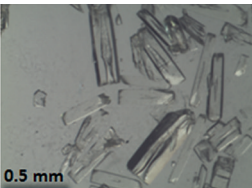
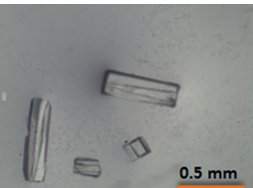
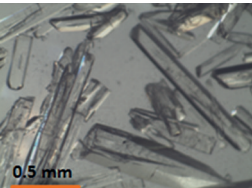
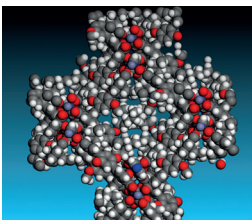
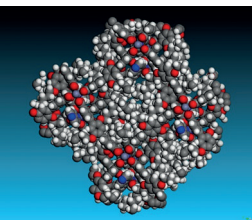
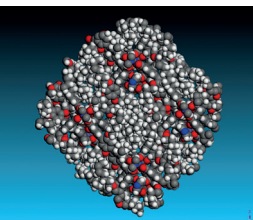
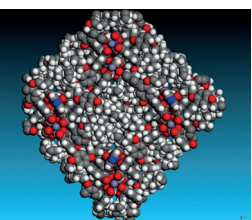
Information). The window size of the clover-shaped channels is gradually reduced as the substituent of the terphenyldicarboxylate is changed from  $-\text{OCH}_3$  to  $-\text{OC}_8\text{H}_{17}$ , as indicated in Table 1. Pores generated in SNU-81–SNU-88 are occupied by the guest solvent molecules, as evidenced by thermogravimetric analysis (TGA) and elemental analysis (EA) data.

The powder XRD (PXRD) patterns measured for as-synthesized samples did not exactly match with those simulated from the X-ray crystallographic data. The peak positions and intensities in SNU-81–SNU-85 were changed, although the PXRD patterns of SNU-86–SNU-88, which contain fewer guest molecules, showed very similar patterns to those derived from the simulation. We assume that changes in the PXRD patterns of SNU-81–SNU-85 are related to structural changes associated with the partial loss of guest solvent molecules during the measurements.

To see the relationship between the hollow-crystal morphology and the framework structure, face-indexing experiments were performed. Interestingly, the hollow axis of a single crystal (Figure 1b) is parallel to the axis of the 1D channels of the MOF (Figure 2a). This suggests that the growth of the present 3D MOFs should be ascribed to the successive unidirectional addition of bpy linkers to the axial sites of the  $\text{Zn}_2$ -paddle-wheel units that belong to the 2D square-grid network.

The formation of hollow tubular crystals mainly depends on the solubility of the ligands.<sup>[11]</sup> For MOFs constructed from less soluble ligands, such as  $\text{H}_2\text{C}^1\text{TPDC}$ ,  $\text{H}_2\text{C}^2\text{TPDC}$ , and  $\text{H}_2\text{C}^3\text{TPDC}$ , hollow crystals were formed from solutions in DMF/EtOH (6:1 v/v) with lower concentrations of reactants (ca. 0.01 M of  $\text{Zn}(\text{NO}_3)_2 \cdot 6\text{H}_2\text{O}$ , 0.007 M of  $\text{H}_2\text{C}^n\text{TPDC}$ , 0.007 M of bpy), whereas non-hollow crystals were often yielded from solutions in DMF/EtOH (4:1 v/v) with higher concentrations of reactants (ca. 0.015 M of  $\text{Zn}(\text{NO}_3)_2 \cdot 6\text{H}_2\text{O}$ , 0.012 M of  $\text{H}_2\text{C}^n\text{TPDC}$ , 0.012 M of

**Table 1.** Morphologies, X-ray structures, PLATON void volumes, and channel sizes of MOFs.

	SNU-81	SNU-82	SNU-83	SNU-84
crystal morphology				
X-ray structure				
PLATON void volume [%]	64	60	58	52
window size of channel [Å] <sup>[a]</sup>	15×4, 15×2	15×1	3×2	2×2
	SNU-85	SNU-86	SNU-87	SNU-88
crystal morphology				
X-ray structure				
PLATON void volume [%]	50	48	46	38
window size of channel [Å] <sup>[a]</sup>	2×0.2	0	0	0

[a] The longest length and shortest width for the clover-shaped channels.

bpy). On the other hand, ligands such as  $\text{H}_2\text{C}^4\text{TPDC}$ ,  $\text{H}_2\text{C}^6\text{TPDC}$ , and  $\text{H}_2\text{C}^8\text{TPDC}$  with better solubility formed hollow crystals of the MOFs, even at high concentrations of the reactants. The ligands with bulkier substituents, such as nonyloxy, decyloxy, and cyclohexylmethoxy derivatives, yielded only precipitates. The present results are significant because the hollow morphology was never found in any MOFs with pillared structures.<sup>[12]</sup> Crystal growth in one direction leads to a needle-like morphology, but a fast crystallization rate with unidirectional crystal growth may create hollow tubular crystals because the diffusion rate of the building units into the crystal channels must be reduced as crystal growth takes place.<sup>[9a]</sup> These are also supported by non-hollow crystals formed from solutions with higher concentrations of reactants, for which the chances of filling the hole are higher. Recently, it was reported that supersaturation of the crystal growth units also played an important role in the morphology control of the crystals.<sup>[13b]</sup> The hollow morphology of the present MOF crystals must result

from a synergetic effect of the longer dicarboxyl ligand incorporating alkoxy pendant groups and an appropriate concentration of reactants.

When the MOFs were activated by using supercritical  $\text{CO}_2$ , the tubular hollow-crystal morphologies were retained, but the crystals were cracked. Therefore, the single-crystal XRD data of the activated samples could not be collected. The PXRD patterns for the activated samples, in particular, for SNU-81–SNU-85, indicated that the structures were altered by activation, compared with those of the as-synthesized samples or the simulated patterns derived from single-crystal X-ray data (see Figures S11–S14 in the Supporting Information). This must be due to the presence of flexible alkoxy pendant groups, as well as the interpenetrated structures, which undergo some movement on removal of the guest solvent molecules from the pores. We tried to determine the unit-cell parameters for these activated samples from their PXRD patterns by using the reflux module of the Materials Studio program (Materials Studio v5.5,

Accelrys Inc., San Diego, CA, 2010), but failed to get any reasonable results.

### Gas Sorption Properties of SNU-81'–SNU-88'

Gas sorption isotherms for all activated MOFs, SNU-81'–SNU-88', were measured for N<sub>2</sub>, H<sub>2</sub>, CO<sub>2</sub>, and CH<sub>4</sub> gases (Table 2).

	SNU-81' [cm <sup>3</sup> g <sup>−1</sup> ] [(mmol g <sup>−1</sup> )]	SNU-82' [cm <sup>3</sup> g <sup>−1</sup> ] [(mmol g <sup>−1</sup> )]
N <sub>2</sub> , 77 K	50.4 (2.25)	25.5 (1.14)
N <sub>2</sub> , 298 K	2.3 (0.10)	0.33 (0.01)
H <sub>2</sub> , 77 K	81.6 (3.64)	46.6 (2.08)
H <sub>2</sub> , 87 K	60.6 (2.71)	37.0 (1.65)
H <sub>2</sub> , 298 K	0.68 (0.03)	0.29 (0.01)
Q <sub>st</sub> (H <sub>2</sub> ) [kJ mol <sup>−1</sup> ]	8.53	6.67
CO <sub>2</sub> , 195 K	110 (4.91)	60 (2.68)
CO <sub>2</sub> , 273 K	40 (1.79)	20 (0.89)
CO <sub>2</sub> , 298 K	29 (1.29)	7.4 (0.33)
Q <sub>st</sub> (CO <sub>2</sub> ) [kJ mol <sup>−1</sup> ]	32.1	30.5
CH <sub>4</sub> , 195 K	51 (2.28)	21 (0.94)
CH <sub>4</sub> , 273 K	16 (0.71)	3.9 (0.17)
CH <sub>4</sub> , 298 K	8.8 (0.39)	1.7 (0.08)
Q <sub>st</sub> (CH <sub>4</sub> ) [kJ mol <sup>−1</sup> ]	20.8	24.2

[a] Gas sorption data at 1 atm for all gases, apart from N<sub>2</sub> (0.9 atm).

Among them, only SNU-81' and SNU-82', with methoxy and ethoxy pendant groups, respectively, adsorb N<sub>2</sub> and H<sub>2</sub> gases at 77 K, as well as CO<sub>2</sub> and CH<sub>4</sub> gases at 195, 273, and 298 K (see Figures S19–S21 in the Supporting Information). In general, SNU-81' with methoxy pendant groups shows higher gas uptake capacities than SNU-82', which incorporates an ethoxy pendant group. At 77 K, SNU-81' and SNU-82' adsorb small amounts of N<sub>2</sub> gas, showing a big hysteresis on desorption (Figures S19 and S20 in the Supporting Information), which might be due to gradual desorption caused by the combination of different pore sizes, that is, multiple pockets (small pores) possibly formed by the interpenetrated structures and flexible pendent chains. Both of the MOFs show slightly higher H<sub>2</sub> gas adsorption than N<sub>2</sub> gas uptake at 77 K and 1 atm. At room temperature, they barely adsorb N<sub>2</sub> and H<sub>2</sub> gases. MOFs SNU-81' and SNU-82' show relatively high CO<sub>2</sub> adsorption capacities at 195, 273, and 298 K, with a slight hysteresis in the desorption process (see Table 2 and Figures S19 and S20 in the Supporting Information). SNU-81' adsorbs 110 (4.91), 40 (1.79), and 29 cm<sup>3</sup> g<sup>−1</sup> (1.29 mmol g<sup>−1</sup>) of CO<sub>2</sub> at 195, 273, and 298 K, respectively, under 1 atm of CO<sub>2</sub>. In the case of SNU-82', which contains one more CH<sub>2</sub> group in the pendant chain, the CO<sub>2</sub> sorption capacities are reduced to nearly half of those in SNU-81'. It adsorbs 60 (2.68), 20 (0.89), and 7.4 cm<sup>3</sup> g<sup>−1</sup> (0.33 mmol g<sup>−1</sup>) of CO<sub>2</sub> at 195, 273, and 298 K, respectively, under 1 atm of CO<sub>2</sub>. The surface areas of SNU-81' and SNU-82', as estimated from the CO<sub>2</sub> adsorption isotherms at 195 K by the Dubinin–Radushkevich (DR) method, are 278 and 212 m<sup>2</sup> g<sup>−1</sup>, respectively. The CH<sub>4</sub> adsorption capacities in SNU-81' and SNU-82' are less than half of the CO<sub>2</sub> adsorption ca-

pacities. The isosteric heats of CO<sub>2</sub> and CH<sub>4</sub> adsorption were calculated by using the Clausius–Clapeyron equation based on their adsorption isotherms at 195, 273, and 298 K, which were fit to the Langmuir–Freundlich equation (see the Supporting Information for a detailed description). The isosteric heats of CO<sub>2</sub> adsorption at low gas loadings in SNU-81' and SNU-82' are 32 and 30 kJ mol<sup>−1</sup>, respectively (Figure S23 in the Supporting Information). The isosteric heats of CH<sub>4</sub> adsorption in SNU-81' and SNU-82' are 21 and 24 kJ mol<sup>−1</sup>, respectively.

As expected, other MOFs with longer pendant groups, SNU-83'–SNU-88', show extremely low gas adsorption capacities compared with those of SNU-81' and SNU-82' (see Figures S24 and S25 in the Supporting Information). Even at 77 K, their N<sub>2</sub> and H<sub>2</sub> adsorption capacities are less than 15 and 23 cm<sup>3</sup> g<sup>−1</sup>, respectively, because most of the pore spaces must be occupied by the pendant chains. The CO<sub>2</sub> adsorption capacities at 298 K and 1 atm are also low, less than 12 cm<sup>3</sup> g<sup>−1</sup>.

To see the effects of the hollow tubular morphology on the gas sorption properties, comparisons of the gas sorption properties between the hollow crystals and non-hollow crystals should be made. However, we were not able to compare them owing to the failure of collecting a sufficient amount of non-hollow crystals. We assume that the hollow and non-hollow crystals would not show different gas sorption properties because it is well known that crystal size, either powder or large crystalline form, has little effect on gas adsorption capacities.

### CO<sub>2</sub> Adsorption Selectivity of SNU-81' and SNU-82'

SNU-81' and SNU-82' exhibit selective CO<sub>2</sub> adsorption properties over H<sub>2</sub>, N<sub>2</sub>, and CH<sub>4</sub> gases at room temperature (Figure 3 and Figure S21 in the Supporting Information). The selectivity values of CO<sub>2</sub> adsorption over CH<sub>4</sub> and N<sub>2</sub> were estimated by

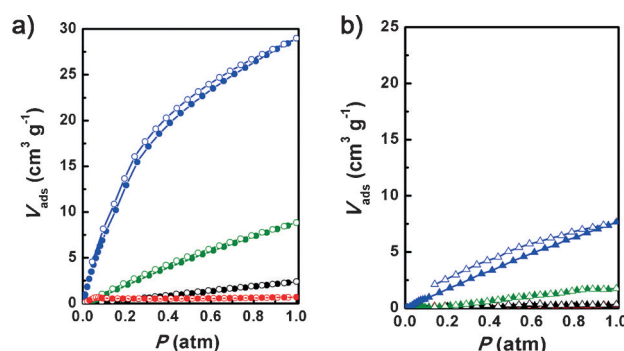


**Figure 3.** Gas adsorption isotherms measured at 298 K for CO<sub>2</sub> (blue), CH<sub>4</sub> (green), N<sub>2</sub> (black), and H<sub>2</sub> (red) gases: a) SNU-81' (circles), and b) SNU-82' (triangles); filled shapes: adsorption, open shapes: desorption.

using vacuum swing adsorption (VSA) separation parameters proposed by Snurr and Bae (see Table S7 in the Supporting Information).<sup>[14]</sup> The CO<sub>2</sub>/CH<sub>4</sub> (1:1) VSA separation parameters at room temperature calculated for SNU-81' and SNU-82' are 7.3 and 2.2, respectively, which are much lower than the highest value (359) for CUK-1.<sup>[14]</sup> However, the CO<sub>2</sub>/N<sub>2</sub> (1:9) VSA separation parameter calculated for SNU-81' (58.6) was relatively

high, although it was lower than the highest value (396) observed for ZIF-78.<sup>[14]</sup> The CO<sub>2</sub>/N<sub>2</sub> (1:9) VSA separation parameters for SNU-82' could not be calculated owing to insufficient data on N<sub>2</sub> adsorption at room temperature.

## Conclusion

A series of 3D porous MOFs, SNU-81–SNU-88, were synthesized from the solvothermal reaction of various alkoxy-substituted (–OC<sub>n</sub>H<sub>2n+1</sub>; *n* = 1–8) *para*-terphenyldicarboxylic acids with bpy and Zn(NO<sub>3</sub>)<sub>2</sub>·6H<sub>2</sub>O in DMF/EtOH. The single crystals of the MOFs have hollow tubular morphologies. The X-ray crystal structures indicate that they have doubly interpenetrated 3D frameworks that generate clover-shaped 1D channels, the window sizes of which gradually reduce as the alkoxy pendant groups are elongated from –OCH<sub>3</sub> to –OC<sub>8</sub>H<sub>17</sub> pendant groups. The face-indexing experiments reveal that the axis of the hollow tube of a crystal is parallel to the 1D channels of the MOF, which suggests a possible growth mechanism of the hollow tubular crystal, that is, unidirectional addition of bpy to the well-formed 2D square-grid network. The control experiments suggested that the hollow morphologies resulted from the long dicarboxylic acid with alkoxy pendant groups, appropriate concentrations of reactants, and fast crystal growth dynamics. Interestingly, among the desolvated frameworks of SNU-81–SNU-88, only SNU-81' and SNU-82' adsorbed CO<sub>2</sub> at room temperature and exhibited high adsorption selectivity for CO<sub>2</sub> over N<sub>2</sub> and CH<sub>4</sub>. This indicates that alkoxy pendant doors of MOFs should have an appropriate length for selective CO<sub>2</sub> capture, and those longer than –OC<sub>2</sub>H<sub>5</sub> are too heavy to open for CO<sub>2</sub> at room temperature.

## Experimental Section

### General

All chemicals used were commercially available and of reagent grade. THF was distilled under nitrogen from sodium benzophenone. NMR spectra were measured on a Bruker Spectrospin 300 spectrometer. EA was performed with a PerkinElmer 2400 Series II CHN analyzer. TGA was performed on a TGA Q50 TA instrument under an N<sub>2</sub> atmosphere at a scan rate of 5 °C min<sup>–1</sup>. PXRD data were recorded on a Bruker New D8 diffractometer at 40 kV and 40 mA for Cu<sub>Kα</sub> (λ = 1.54050 Å) with a scan speed of 6° min<sup>–1</sup> at 298 K for the powdered flat samples, to which a small amount of mother liquor was added.

### Synthesis of Ligands

A series of *para*-terphenyldicarboxylic acids with various alkoxy substituents (H<sub>2</sub>C<sup>1</sup>TPDC; *n* = 1–8) were synthesized by the Suzuki–Miyaura cross-coupling reactions of the respective 1,4-dibromo-2,5-dialkoxybenzene with 4-(methoxycarbonyl)phenylboronic acid (see the Supporting Information for details of synthetic procedures and Tables S1–S3 for characterization data).

### Synthesis of SNU-81

Zn(NO<sub>3</sub>)<sub>2</sub>·6H<sub>2</sub>O (0.020 g, 0.065 mmol), H<sub>2</sub>C<sup>1</sup>TPDC (0.019 g, 0.050 mmol), and bpy (0.008 g, 0.050 mmol) were dissolved in

a mixture of DMF (6 mL) and EtOH (1 mL) in a glass serum bottle, which was capped with a silicon stopper and aluminum seal, and then heated at 80 °C for 24 h in a programmable furnace. Pale-yellow, hollow, tubular crystals resulted, along with a few non-hollow crystals. The crystals were filtered off and washed with DMF. Yield: 0.025 g, 50%; elemental analysis calcd (%) for C<sub>92</sub>H<sub>130</sub>N<sub>14</sub>O<sub>25</sub>Zn<sub>2</sub>: C 56.29, H 6.68, N 9.99; found: C 55.96, H 6.46, N 9.70.

### Syntheses of SNU-82–SNU-88

All MOFs were synthesized by similar procedures to that used for SNU-81. The reaction conditions, yields, and EA results for these MOFs are presented in Table S4 in the Supporting Information.

### X-ray Crystallography

X-ray single-crystal data were collected on an Enraf Nonius Kappa CCD diffractometer by using graphite-monochromated Mo<sub>Kα</sub> radiation (λ = 0.71073 Å) at 295 K. The data were collected for a whole crystal without cutting. Each crystal was sealed in a glass capillary together with the mother liquor, and the hollow space in the crystal was also filled with the mother liquor. Preliminary orientation matrices and unit-cell parameters were obtained from the peaks of the first 10 frames and then refined by using the whole data set. Frames were integrated and corrected for Lorentz and polarization effects by using the DENZO program.<sup>[15]</sup> The scaling and global refinement of crystal parameters were performed by using the SCALEPACK program.<sup>[15]</sup> The structure was solved by using the SHELXS-97<sup>[16]</sup> program, and full-matrix least-squares refinement against *F*<sup>2</sup> was carried out by using the SHELXL-97 program.<sup>[16]</sup> All hydrogen atoms were assigned on the basis of geometrical considerations and allowed to ride on the respective carbon atoms. The solvent molecules could not be located from the difference maps, and the residual electron density corresponding to the solvent molecules were ignored by using the SQUEEZE<sup>[17]</sup> option of PLATON.<sup>[18]</sup> The pendent alkyl groups had high thermal disorder because the structures were solved by using data collected at 298 K. However, the XRD data collected at 100 K could not be solved, except for SNU-88, owing to the poor quality of the data. The position constraints were applied for the central benzene ring of the dicarboxylate linkers as well as the pendent alkoxy groups and refined isotropically. The exact positions of the pendent alkyl chains were located in the case of SNU-81 – SNU-83, with shorter pendent arms, but for those with longer alkoxy chains (*n* > 4) the carbon atom positions were highly disordered. The presence of high static disorder in the central benzene ring of the dicarboxylate linkers and alkoxy pendants generated numerous A- and B-type alerts on the cif check, which could not be resolved better. The X-ray crystallographic data are presented in Table 3 and Table S5 and S6 in the Supporting Information.

CCDC 986077 (SNU-81), 986078 (SNU-82), 986079 (SNU-83), 986080 (SNU-84), 986081 (SNU-85), 986082 (SNU-86), 986083 (SNU-87) and 986084 (SNU-88) contain the supplementary crystallographic data for this paper. These data are provided free of charge by The Cambridge Crystallographic Data Centre.

### Face Indexing

Face indexing was performed for a hollow tubular crystal sealed in a capillary on an Enraf Nonius Kappa CCD diffractometer at room temperature by using Bruker AXS SuperGUI software. It was found that the direction of the hollow tube of the crystal coincided with

Table 3. Crystallographic data for SNU-81 and SNU-82.

	SNU-81	SNU-82
formula	C <sub>54</sub> H <sub>40</sub> N <sub>2</sub> O <sub>12</sub> Zn <sub>2</sub>	C <sub>58</sub> H <sub>48</sub> N <sub>2</sub> O <sub>12</sub> Zn <sub>2</sub>
<i>M<sub>r</sub></i>	1039.62	1095.72
crystal system	monoclinic	monoclinic
space group	C2/c	C2/c
<i>a</i> [Å]	28.0682(7)	39.0045(10)
<i>b</i> [Å]	27.1147(6)	27.4307(7)
<i>c</i> [Å]	28.0603(5)	27.3625(7)
$\beta$ [°]	98.558(1)	133.835(1)
<i>V</i> [Å <sup>3</sup> ]	21117.8(8)	21117.6(9)
<i>Z</i>	8	8
<i>T</i> [K]	295	295
GOF ( <i>F</i> <sup>2</sup> )	0.812	1.099
<i>R<sub>i</sub></i> [ <i>I</i> > 2σ( <i>I</i> )] <sup>[a]</sup>	0.0721	0.0817
<i>wR<sub>2</sub></i> [ <i>I</i> > 2σ( <i>I</i> )] <sup>[b]</sup>	0.1962	0.2477

[a]  $R_1 = \sum(|F_o| - |F_c|) / \sum|F_o|$ ; [b]  $wR_2 = [\sum w(F_o^2 - F_c^2)^2 / \sum w(F_o^2)^2]^{1/2}$ ;  $w = 1 / [\sigma^2(F_o^2) + (AP)^2 + (BP)]$ ,  $P = (F_o^2 + 2F_c^2)/3$ ;  $A = 0.0805$ ,  $B = 0.0000$  for SNU-81; and  $A = 0.1114$ ,  $B = 0.0000$  for SNU-82.

the *a*\* axis (perpendicular to the *bc* plane) of the unit cell for SNU-81–SNU-88.

### Activation of MOFs with Supercritical CO<sub>2</sub>

The crystals of as-synthesized MOFs (ca. 0.1 g) were placed inside the supercritical dryer together with DMF, and the drying chamber was sealed. The temperature and pressure of the chamber were increased to 40 °C and 200 bar with CO<sub>2</sub>. The chamber was vented at a rate of 10 mL min<sup>−1</sup> and then filled with CO<sub>2</sub> again. The cycles of refilling with CO<sub>2</sub>, pressurizing, and venting were repeated for 24 h. After drying, the closed container was transferred to a glove box filled with argon and transferred to a gas sorption cell. SNU-81: Elemental analysis calcd (%) for C<sub>54</sub>H<sub>40</sub>N<sub>2</sub>O<sub>12</sub>Zn<sub>2</sub>: C 62.38, H 3.88, N 2.69; found: C 62.35, H 3.89, N 2.70. SNU-82: Elemental analysis calcd (%) for C<sub>58</sub>H<sub>48</sub>N<sub>2</sub>O<sub>12</sub>Zn<sub>2</sub>: C 63.57, H 4.42, N 2.56; found: C 63.30, H 4.28, N 2.52.

### Gas Sorption Measurements

Gas adsorption–desorption measurements were performed by using Autosorb-1 or Autosorb-3B (Quantachrome Instruments) apparatus up to 1 atm. All gases used in the studies were of 99.999% purity. The gas sorption isotherms were measured after the activated samples with supercritical CO<sub>2</sub> were reactivated at room temperature under high vacuum in the gas sorption cells. Before and after gas sorption measurements, the sample weight was measured precisely.

### Calculation of Isosteric Heats of CO<sub>2</sub> and CH<sub>4</sub> Adsorption

The CO<sub>2</sub> and CH<sub>4</sub> gas adsorption isotherms at 195, 273, and 298 K were fitted with a Langmuir–Freundlich equation [Eq. (1)]. The isosteric heats of CO<sub>2</sub> and CH<sub>4</sub> adsorption were calculated from isotherms fitted to Equation (1) by using the Clausius–Clapeyron expression [Eq. (2)], in which *P* is pressure (atm), *N* is the amount of adsorbed gas (mmol g<sup>−1</sup>), *N<sub>m</sub>* is the amount adsorbed gas at saturation, and *b* and *c* are constants.

$$N = \frac{N_m b P^{(1/c)}}{1 + b P^{(1/c)}} \quad (1)$$

$$(\ln P)_N = -\frac{Q_{st}}{R} \frac{1}{T} + C \quad (2)$$

### Calculation of Selectivity

Because calculation of selectivity from the adsorption isotherms of the gas mixture could not be measured due the difficulty of setting up the dedicated instruments, numerical methods proposed by Snurr and Bae<sup>[14]</sup> were performed to calculate the VSA separation parameters. Because the current MOFs are highly flexible owing to the alkoxy pendant groups and interpenetrated structures, the selectivity calculation methods that are applicable to rigid porous materials, such as the calculation from single-component isotherms, Henry constants, and ideal adsorbed solution theory (IAST), have not been performed.

### Calculation of VSA Separation Parameters

To evaluate materials for the separation of CO<sub>2</sub> from CH<sub>4</sub> and N<sub>2</sub> by the VSA method, we estimated five parameters suggested by Bae and Snurr:<sup>[14]</sup> 1) CO<sub>2</sub> uptake under the adsorption conditions, *N*<sub>1</sub><sup>ads</sup> (mol kg<sup>−1</sup>); 2) working CO<sub>2</sub> capacity, Δ*N*<sub>1</sub> = *N*<sub>1</sub><sup>ads</sup> − *N*<sub>1</sub><sup>des</sup> (mol kg<sup>−1</sup>); 3) regenerability, *R* = (Δ*N*<sub>1</sub>/*N*<sub>1</sub><sup>ads</sup>) × 100 (%); 4) selectivity under adsorption conditions, α<sub>12</sub><sup>ads</sup> = (*N*<sub>1</sub><sup>ads</sup>/*N*<sub>2</sub><sup>ads</sup>)(*y*<sub>2</sub>/*y*<sub>1</sub>); and 5) sorbent selection parameter, *S* = (α<sub>12</sub><sup>ads</sup>)<sup>2</sup>/(α<sub>12</sub><sup>des</sup>)(Δ*N*<sub>1</sub>/Δ*N*<sub>2</sub>). *N* is the adsorbed amount and *y* is the mole fraction in the gas phase. Subscripts 1 and 2 indicate the strongly (CO<sub>2</sub>) and weakly adsorbed components (CH<sub>4</sub> or N<sub>2</sub>), respectively. The selectivity parameters were extracted from the isotherms of CO<sub>2</sub>, CH<sub>4</sub>, and N<sub>2</sub> at 298 K, which were fit to Equation (1). The results are presented in Table S7 in the Supporting Information.

### Acknowledgements

This work was supported by National Research Foundation of Korea (NRF) Grant funded by the Korean Government (NRF-2005-0093842).

**Keywords:** carbon dioxide capture • crystal growth • crystal morphology • gas separation • metal–organic frameworks

- [1] See reviews in the special issue on MOFs: a) M. P. Suh, H. J. Park, T. K. Prasad, D.-W. Lim, *Chem. Rev.* **2012**, *112*, 782–835; b) K. Sumida, D. L. Rogow, J. A. Mason, T. M. McDonald, E. D. Bloch, Z. R. Herm, T.-H. Bae, J. R. Long, *Chem. Rev.* **2012**, *112*, 724–781; c) J.-R. Li, J. Sculley, H.-C. Zhou, *Chem. Rev.* **2012**, *112*, 869–932; d) L. E. Kreno, K. Leong, O. K. Farha, M. Allendorf, R. P. Van Duyne, J. T. Hupp, *Chem. Rev.* **2012**, *112*, 1105–1125; e) special issue: *Chem. Soc. Rev.* **2014**, *43*, 5403–6176.
- [2] a) H.-S. Choi, M. P. Suh, *Angew. Chem. Int. Ed.* **2009**, *48*, 6865–6869; *Angew. Chem.* **2009**, *121*, 6997–7001; b) D. M. D'Alessandro, B. Smit, J. R. Long, *Angew. Chem. Int. Ed.* **2010**, *49*, 6058–6082; *Angew. Chem.* **2010**, *122*, 6194–6219; c) S. D. Kenarsari, D. Yang, G. Jiang, S. Zhang, J. Wang, A. G. Russell, Q. Weif, M. Fane, *RSC Adv.* **2013**, *3*, 22739–22773.
- [3] a) T. K. Kim, M. P. Suh, *Chem. Commun.* **2011**, *47*, 4258–4260; b) D. H. Hong, M. P. Suh, *Chem. Commun.* **2012**, *48*, 9168–9170; c) D. H. Hong, M. P. Suh, *Chem. Eur. J.* **2014**, *20*, 426–434.
- [4] a) S. Henke, R. A. Fischer, *J. Am. Chem. Soc.* **2011**, *133*, 2064–2067; b) S. Henke, R. Schmid, J.-D. Grunwaldt, R. A. Fischer, *Chem. Eur. J.* **2010**, *16*, 14296–14306; c) Z.-J. Lin, J. Lü, M. Hong, R. Cao, *Chem. Soc. Rev.* **2014**, *43*, 5867–5895; d) A. Schneemann, V. Bon, I. Schwedler, I. Senkovska, S. Kaskel, R. A. Fischer, *Chem. Soc. Rev.* **2014**, *43*, 6062–6096.

- [5] C. Y. Lee, Y.-S. Bae, N. C. Jeong, O. K. Farha, A. A. Sarjeant, C. L. Stern, P. Nickias, R. Q. Snurr, J. T. Hupp, S. T. Nguyen, *J. Am. Chem. Soc.* **2011**, *133*, 5228–5231.
- [6] a) R. A. Schoonheydt, *Angew. Chem. Int. Ed.* **2008**, *47*, 9188–9191; *Angew. Chem.* **2008**, *120*, 9328–9331; b) M. B. J. Roelfaers, R. Ameloot, M. Baruah, H. Uji-i, M. Bulut, G. D. Cremer, U. Muller, P. A. Jacobs, J. Hofkens, B. F. Sels, D. E. De Vos, *J. Am. Chem. Soc.* **2008**, *130*, 5763–5772; c) M. Y. Masoomi, S. Beheshti, A. Morsali, *Cryst. Growth Des.* **2015**, *15*, 2533–2538.
- [7] N. Stock, S. Biswas, *Chem. Rev.* **2012**, *112*, 933–969.
- [8] a) A. Umemura, S. Diring, S. Furukawa, H. Uehara, T. Tsuruoka, S. Kitagawa, *J. Am. Chem. Soc.* **2011**, *133*, 15506–15513; b) T. Tsuruoka, S. Furukawa, Y. Takashima, K. Yoshida, S. Isoda, S. Kitagawa, *Angew. Chem. Int. Ed.* **2009**, *48*, 4739–4743; *Angew. Chem.* **2009**, *121*, 4833–4837.
- [9] a) G. Mouchaham, N. Roques, A. Kaiba, P. Guionneau, J.-P. Sutter, *CrytEngComm* **2010**, *12*, 3496–3498; b) H. Li, M. Eddaoudi, M. O’Keeffe, O. M. Yaghi, *Nature* **1999**, *402*, 276–279; c) Y. Yan, X. Lin, S. Yang, A. J. Blake, A. Dailly, N. R. Champness, P. Hubberstey, M. Schroder, *Chem. Commun.* **2009**, 1025–1027.
- [10] a) J. Cohen, R. A. Henry, S. Skolnik, G. B. L. Smith, *Science* **1950**, *111*, 278–279; b) W. F. Seip, F. W. Barnes, Jr., *Science* **1960**, *131*, 161–161.
- [11] The solubility of H<sub>2</sub>C<sup>18</sup>TPDC in DMF increases roughly as *n* increases.
- [12] a) B.-Q. Ma, K. L. Mulfort, J. T. Hupp, *Inorg. Chem.* **2005**, *44*, 4912–4914; b) B. Chen, C. Liang, J. Yang, D. S. Contreras, Y. L. Clancy, E. B. Lobkovsky, O. M. Yaghi, S. Dai, *Angew. Chem. Int. Ed.* **2006**, *45*, 1390–1393; *Angew. Chem.* **2006**, *118*, 1418–1421; c) T. Gadzikwa, B.-S. Zeng, J. T. Hupp, S. T. Nguyen, *Chem. Commun.* **2008**, 3672–3674.
- [13] H.-x. Lin, Z.-c. Lei, Z.-y. Jiang, C.-p. Hou, D.-y. Liu, M.-m. Xu, Z.-q. Tian, Z.-x. Xie, *J. Am. Chem. Soc.* **2013**, *135*, 9311–9314.
- [14] Y.-S. Bae, R. Q. Snurr, *Angew. Chem. Int. Ed.* **2011**, *50*, 11586–11596; *Angew. Chem.* **2011**, *123*, 11790–11801.
- [15] Z. Otwinowski, W. Minor in *Methods in Enzymology*, Vol. 276 (Eds.: C. W. Carter, Jr., R. M. Sweet), Academic Press, San Diego, **1997**, p. 307–326.
- [16] SHELX97, Programs for Crystal Structure Analysis (Release 97–92), G. M. Sheldrick, Institut für Anorganische Chemie der Universität Göttingen, Göttingen (Germany), **1998**.
- [17] P. van der Sluis, A. L. Spek, *Acta Crystallogr. Sect. A* **1990**, *46*, 194–201.
- [18] a) A. L. Spek, *Acta Crystallogr. Sect. A* **1990**, *46*, C34; b) A. L. Spek, PLATON, A Multipurpose Crystallographic Tool, Utrecht University, Utrecht (The Netherlands), **1998**.

Manuscript received: April 2, 2015

Revised: May 29, 2015

Accepted Article published: June 25, 2015

Final Article published: July 30, 2015